Polymer 51 (2010) 5245–5254

Contents lists available at ScienceDirect

Polymer

journal homepage: www.elsevier.com/locate/polymer

Dynamic relaxation characteristics of polymer nanocomposites based on poly(ether imide) and poly(methyl methacrylate)

A.C. Comer, A.L. Heilman, D.S. Kalika*

Department of Chemical and Materials Engineering, University of Kentucky, Lexington, KY 40506-0046, United States

ARTICLE INFO

Article history:
Received 14 July 2010
Received in revised form
20 August 2010
Accepted 25 August 2010
Available online 16 September 2010

Keywords:
Glass transition
Dynamic mechanical analysis
Dielectric spectroscopy

ABSTRACT

The dynamic relaxation characteristics of poly(ether imide) and poly(methyl methacrylate) nanocomposites based on native and surface-modified (i.e., hydrophobic) fumed silicas were investigated by dynamic mechanical analysis and dielectric spectroscopy. The nanocomposites displayed a dual glass transition behavior in the dynamic mechanical studies encompassing a bulk polymer glass transition (close to T_g for the unfilled polymer), and a second, higher-temperature transition reflecting relaxation of polymer chain segments constrained owing to their proximity to the particle surface. The position and intensity of the higher-temperature transition varied with particle loading and surface chemistry, and reflected the relative populations of segments constrained or immobilized at the particle-polymer interface. Dielectric measurements, which were used to probe the time–temperature response across the local sub-glass relaxations, indicated no variation in relaxation characteristics with particle loading.

1. Introduction

Polymer nanocomposites, i.e. inorganic-organic hybrid materials that contain nanoscale filler with characteristic dimensions at or below 100 nm, have been the subject of extensive study owing to their potentially superior performance properties as compared to conventional filled plastics. Over the last two decades, a broad body of experimental and theoretical work has emerged that explores the relationships between filler size and geometry, surface chemistry, and nanocomposite morphology and their influence on ultimate performance characteristics; many aspects of this work have been summarized in the numerous review papers available in the literature [1–9].

An important factor in understanding the potential enhancement of bulk properties in polymer nanocomposites is the extent to which the presence of nanoscale filler alters the characteristics of the surrounding polymer matrix phase [9]. The introduction of spherical nanoscale particles, for example, leads to the creation of vast amounts of particle-polymer surface area that can strongly influence polymer chain mobility in the vicinity of the solid-polymer interface. The quality of particle-polymer interactions, as well as physical confinement effects, are often manifested by shifts in the glass transition temperature (T_g), as well as changes in the underlying time–temperature characteristics of the glass–rubber and sub-glass relaxation processes [10]. In situations where favorable interactions are established between the nanoparticles and the polymer matrix, positive offsets in T_g are typically observed, as well as the possible appearance of a second, higher T_g corresponding to the presence of a distinct, constrained population of chain segments in the vicinity of the particle surface [11–18]. For particle-polymer combinations with poor wetting characteristics, reductions in T_g with nanoparticle loading have been reported [19–22].

In this study, we examine the dynamic relaxation characteristics of glassy polymer nanocomposites based on amorphous poly(ether imide) [PEI] and poly(methyl methacrylate) [PMMA] filled with fumed silica nanoparticles. Four series of PEI composites are investigated, encompassing native SiO_2 particles, and three commercial silicas produced with various surface treatments intended to render them hydrophobic in character. The preparation and morphology of the PEI composites were previously described by Takahashi and Paul, who explored the relationships between particle dispersion, potential internal void formation and gas transport properties as a function of nanoparticle loading and surface chemistry [23,24]. In the current work, we assess the influence of the particles on the glass–rubber and sub-glass relaxations of PEI and PMMA composites using dynamic mechanical and dielectric spectroscopy methods. Of particular interest is the observation of dual glass–rubber relaxations in these composites, a behavior discussed by Tsagaropoulos and Eisenberg [13,14]. In their study on a variety of favorably-interacting polymer-silica systems, Tsagaropoulos and Eisenberg saw that silica particle (7 nm diameter) loadings on the order of

* Corresponding author. Tel.: +1 859 257 5507; fax: +1 859 323 1929.
E-mail address: kalika@engr.uky.edu (D.S. Kalika).

0032-3861/$ – see front matter © 2010 Elsevier Ltd. All rights reserved.
doi:10.1016/j.polymer.2010.08.053

10 wt% and higher led to the emergence of two distinct T_g events as measured by dynamic mechanical analysis: a bulk T_g corresponding to the glass transition of the unfilled polymer, and a second, higher T_g offset by ~40–100 °C. The relative intensity and position of these relaxations were interpreted according to the overall loading of the nanoparticles, and the respective populations of loosely-bound and more tightly-bound polymer segments near the particle surface. In the work presented here, the generality of the dual-T_g response will be considered for both the PEI- and PMMA-based composites, as well as any potential perturbation of the sub-glass relaxations measured for these systems.

2. Experimental

2.1. Materials

Poly(ether imide) [PEI] resin pellets were obtained from GE Plastics (Ultem® 1000). Poly(methyl methacrylate) [PMMA] pellets were obtained from Altuglas International (Plexiglas® V826). Silica nanoparticles (99.5% purity; 10 nm diameter) were purchased from Aldrich, with a reported BET surface area of 590–690 m^2/g and density of 2.2 g/cm^3. Commercial fumed silicas with modified surfaces were obtained from Cabot Corporation: Cab-o-sil® TS-530, TS-610, and TS-720. The surface chemistry for each of these nanoparticles is presented in Table 1, and details on particle properties are provided in Ref. [23]. The series of particles encompasses nominal diameters from ~10 to 30 nm, with corresponding densities of 2.2 (TS-530), 2.2 (TS-610) and 1.8 g/cm^3 (TS-720), respectively. Solvents used for nanocomposite preparation (dichloromethane; dimethylformamide) were purchased from Fisher Scientific.

Table 1
Surface chemistry of fumed silica nanoparticles. (a) TS-530; (b) TS-610; (c) TS-720.

a

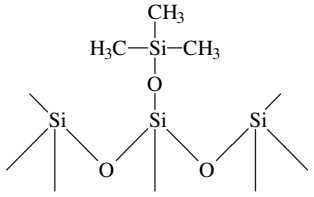

b

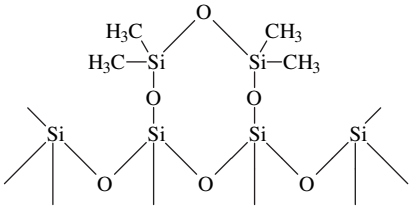

c

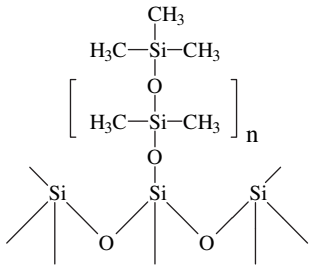

2.2. Sample preparation

2.2.1. PEI-based nanocomposites

PEI pellets (10 wt%) were dissolved in dichloromethane by magnetic stirring at room temperature for 1 h. Nanoparticles in appropriate proportion were added to the polymer solution and subject to vigorous mechanical mixing for 10 min; the blend was then poured into an open, shallow container and solvent was allowed to evaporate at ambient conditions for ~24 h. The resulting composites were placed under vacuum and held at 100 °C (24 h), 200 °C (24 h), and then briefly above T_g (220 °C; 30 min) to ensure full removal of solvent. Finally, the samples were consolidated via compression molding to achieve uniform films of desired thickness. Molding temperatures ranged from 260 to 320 °C depending on filler loading, with melt exposure times <5 min. Film thickness was ~0.7 mm for dynamic mechanical specimens and ~0.3 mm for samples prepared for dielectric measurement. The precise thickness of each film was determined using a digital micrometer with precision to ±1 μm.

2.2.2. PMMA-based nanocomposites

PMMA pellets (10 wt%) were dissolved in DMF by magnetic stirring, followed by addition of an appropriate proportion of nanoparticles; only a single series of PMMA composites was investigated, based on inclusion of the TS-610 particles. The nanocomposite formulations were recovered via precipitation: the polymer/particle solution was poured into a running laboratory blender filled with water, and the precipitated blend was filtered as a coarse powder. Samples were then dried under vacuum at 70 °C (24 h), 110 °C (4 h), and 130 °C (30 min) to facilitate removal of water and residual DMF. Compression molding (220 °C) was used to produce uniform films for dynamic mechanical (0.7 mm) and dielectric (0.3 mm) studies.

2.3. Film density

Bulk density measurements of PEI nanocomposite films were conducted by hydrostatic weighing at 25 °C using a conventional density determination kit (Denver Instruments); deionized ultrafiltered water (Fisher Sci.) was employed as the auxiliary liquid. A minimum of three replicate measurements was completed for each sample tested.

2.4. Dynamic mechanical analysis

Dynamic mechanical analysis was performed using a TA Instruments Q800 DMA configured in tensile geometry. Storage modulus (E') and loss tangent ($\tan\delta$) were recorded both in temperature sweep mode (1 Hz; 3 °C/min) and frequency sweep mode (0.1–30 Hz) at temperatures ranging from 150 to 350 °C (PEI-based films) and 35 to 260 °C (PMMA-based films). All measurements were performed under nitrogen atmosphere.

2.5. Broadband dielectric spectroscopy

Dielectric measurements were conducted using the Novocontrol Broadband Dielectric Spectrometer. To promote electrical contact during measurement, concentric 33 mm diameter silver electrodes were applied to each sample film using a VEECO thermal evaporation system. Samples were subsequently mounted between gold platens and positioned in the Novocontrol Quatro Cryosystem. Dielectric constant (ε') and loss (ε'') were recorded at discrete temperatures ranging from −150 to 380 °C (PEI-based films) and −120° to 230 °C (PMMA-based films). Test frequencies ranged from 0.1 Hz to 3 MHz.

3. Results and discussion

3.1. Nanocomposite density

The incorporation of nanoscale particles into a polymer matrix provides a range of variables that can be exploited for the enhancement of material properties. A crucial aspect of nanocomposite performance is the dispersion of the filler particles within the polymer matrix, as polymer nanocomposites are susceptible to particle agglomeration and potential network formation [25]. Extensive agglomeration within the matrix, accompanied by polymer de-wetting at the particle surface, may lead to the entrapment of voids and defects. Takahashi and Paul recently addressed this issue for a series of PEI-based composites incorporating commercially-available fumed silicas with chemical surface modifications intended to render the particles more hydrophobic in character and thereby more compatible with the PEI matrix [23,24]. Detailed electron microscopy studies revealed moderate to high levels of particle agglomeration in both solution-cast and melt-processed PEI nanocomposites [23]. The morphology of these composites was correlated with bulk density measurements intended to assess the potential formation of internal voids as related to processing history and particle-polymer interaction.

For the studies reported here, we have prepared PEI nanocomposites using components identical to those employed by Takahashi and Paul. Density results for our composites are presented as a function of particle loading in Fig. 1, and are compared to densities predicted based on strict volume additivity (see solid lines in Fig. 1). The density of unfilled PEI was measured as 1.27 g/cm^3, which is in agreement with the value reported by the manufacturer [26]. Fig. 1a presents nanocomposite results for native SiO_2 and the TS-530 and TS-610 particles ($\rho_F = 2.2$ g/cm^3), while Fig. 1b presents results for composites containing TS-720 ($\rho_F = 1.8$ g/cm^3).

Examination of Fig. 1 shows that the PEI composites based on inclusion of TS-610 and TS-720 adhere closely to the volume additivity prediction for loadings up to 20 wt% filler. The results for the TS-610 composites are in close agreement with data reported by Takahashi and Paul, who observed the best overall dispersion quality for the TS-610 particles [23]. Density values for the composites containing TS-530 and native SiO_2 display negative deviations from additivity that increase with particle loading, and that suggest the entrapment of voids or gaps within the composite. For the highest particle loadings, a maximum void volume fraction of apx. 3% is indicated, again consistent with the results reported in Ref. [23].

3.2. PEI composites – dynamic mechanical analysis

Dynamic mechanical results (E'; tanδ vs. temperature) for the series of composites based on PEI and TS-610 particles are presented in Fig. 2. Across the glassy region, the introduction of nanoscale filler leads to a progressive increase in storage modulus, with E' increasing by a factor of two for a loading of 30 wt% particles. At loadings $\geq$ 15 wt%, a two-step incremental drop in modulus is evident with increasing temperature that is indicative of a dual-T_g response, and the plateau modulus that is obtained at the highest measurement temperatures shows a strong positive

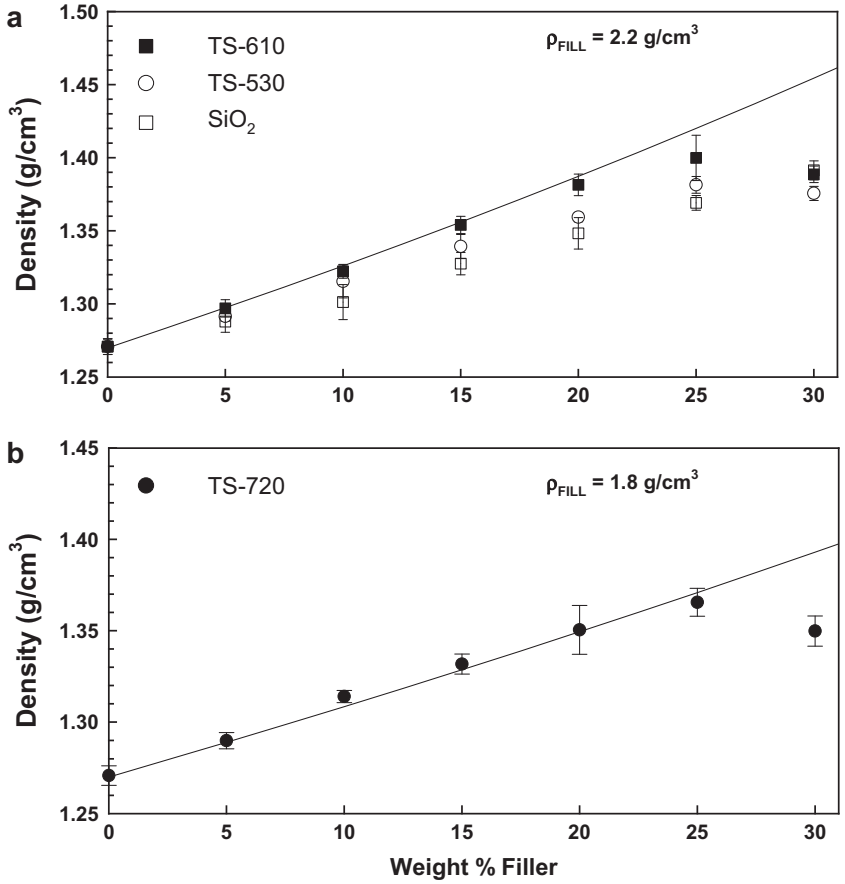

Fig. 1. Density (g/cm^3) vs. weight percent filler for PEI nanocomposites. Solid curves correspond to volume additivity prediction. (a) Filler density = 2.2 g/cm^3 [TS-610; TS-530; SiO_2]; (b) Filler density = 1.8 g/cm^3 [TS-720].

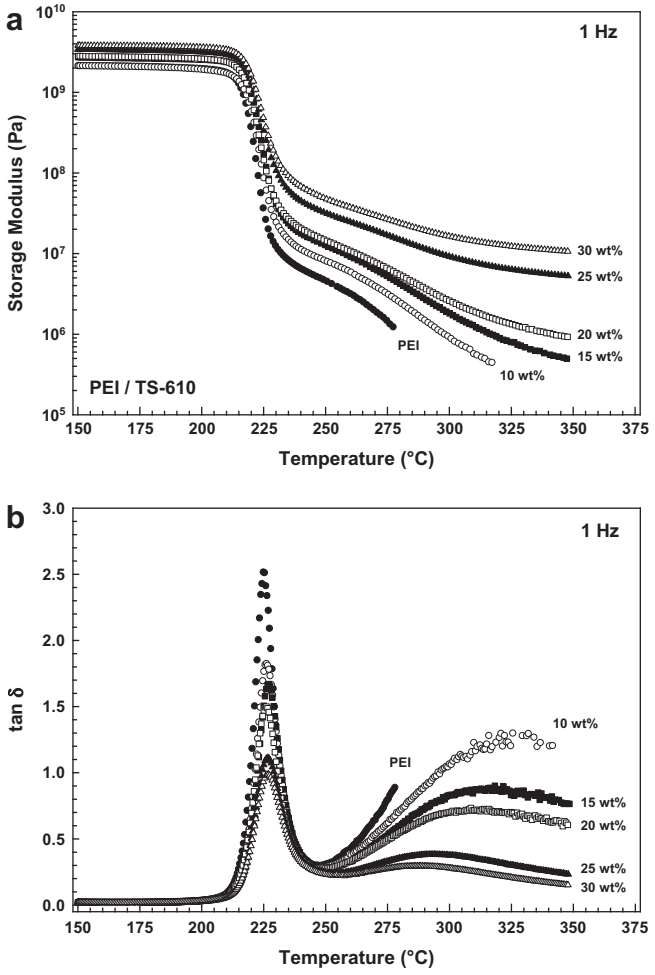

Fig. 2. Dynamic mechanical properties vs. temperature (°C) for PEI/TS-610 nanocomposites. (a) storage modulus (Pa); (b) tanδ. Frequency of 1 Hz; heating rate of 3 °C/min.

correlation with particle loading. Examination of the tanδ results for this series reveals a sharp "bulk polymer" glass transition peak at ~225 °C (T_{g1}); the peak intensity decreases systematically with particle loading, but the position of the peak is nearly invariant across the range of composite compositions studied. At higher temperatures, a broad maximum in tanδ is indicated, suggesting a second glass–rubber relaxation process (T_{g2}) corresponding to the motional response of polymer chain segments impeded to some degree owing to their proximity to the nanoparticle surface. The intensity of this higher-temperature relaxation event decreases with increasing filler content, and the position of the maximum in tanδ shifts to lower temperatures with increased loading. It should be noted that the results for unfilled PEI presented in Fig. 2 correspond to a sample prepared via the same solution-based process used for the nanocomposite specimens. Comparison of these data with dynamic mechanical results obtained for an exclusively melt-processed PEI sample showed no difference in the modulus or tanδ curves, indicating that the drying protocol performed during sample preparation was sufficient in removing residual solvent that could plasticize the matrix and thereby shift T_{g1} to lower temperatures. A summary of tanδ peak temperatures (1 Hz) for the various composites is provided in Table 2.

The trends in dynamic mechanical data for the PEI/TS-610 composites show numerous similarities to the dual-T_g behavior reported by Tsagaropoulos and Eisenberg, and can be satisfactorily

Table 2
Glass transition temperatures for PEI/nanoparticle composites as a function of particle loading (wt%). T_g values correspond to maxima in dynamic mechanical tanδ at a frequency of 1 Hz.

	TS-530		TS-610		TS-720	
wt% filler	T_{g1} [°C]	T_{g2} [°C]	T_{g1} [°C]	T_{g2} [°C]	T_{g1} [°C]	T_{g2} [°C]
0	224	–	224	–	224	–
10	226	321	226	325	226	306
15	226	305	227	316	226	297
20	227	293	226	313	226	287
25	226	289	227	293	224	283
30	226	291	227	289	224	279

explained according to the qualitative model that they proposed [14]. Specifically, it is suggested that the glass–rubber relaxation response of the polymer composites is governed by the distribution of polymer chain segments across three relaxation environments: bulk polymer (essentially unperturbed by the presence of the nanoparticles), loosely-bound polymer, and tightly-bound polymer immobilized at the particle surface. T_{g1} corresponds to the glass transition response involving bulk polymer that is only minimally impacted by inclusion of the particles; the decrease in tanδ peak intensity with increasing loading (T_{g1}) reflects not only the replacement of polymer with solid filler, but also the transformation of some fraction of the surrounding polymer matrix into loosely- and tightly-bound populations. The segmental relaxation of the loosely-bound population (i.e., polymer chain segments hindered by their proximity to the particle surface as well as potential physical confinement effects) is reflected in the higher-temperature relaxation event, T_{g2}. In addition, it is postulated that a subset of polymer segments, the tightly-bound population, is so strongly constrained at the particle surface that these segments are unable to undergo the large-scale motions inherent to the glass–rubber relaxation. The relative position and intensity of the T_{g2} event reflect the progressive transformation of loosely-bound polymer to tightly-bound polymer with increased overall loading: as particle content increases (and average interparticle distance decreases), growing local constraints reduce the relative fraction of loosely-bound segments capable of participating in the glass–rubber relaxation process. This is manifested in an overall decrease in T_{g2} relaxation intensity with increased loading, as well as a shift in peak position to lower temperatures, as the most restricted of the loosely-bound segments are converted into tightly-bound polymer.

Dynamic mechanical results for the PEI composites based on native SiO_2 particles are presented in Fig. 3. As compared to the PEI/TS-610 series, the PEI/SiO_2 composites display a lower overall degree of mechanical reinforcement, especially at loadings $\leq$ 20 wt % SiO_2. The dual-T_g response behavior that is clearly established in the PEI/TS-610 samples at 15 wt% loading is not fully evident in the PEI/SiO_2 composites until a loading of at least 25 wt%. This may indicate a lower degree of particle dispersion across the PEI/SiO_2 series, and potentially weaker interaction between the PEI matrix and the unmodified SiO_2 surface. As reported in Fig. 1, density data for the PEI/SiO_2 series show the strongest negative deviation from volume additivity amongst the various PEI composites, possibly reflecting a lower degree of compatibility (and hence greater agglomeration and void formation) between the PEI thermoplastic and the hydrophilic particles.

A comparison of the dynamic mechanical curves for the four PEI-based nanocomposites is presented in Fig. 4 (15 wt% filler loading). Across the data sets, there is minimal variation in the characteristics of the bulk polymer glass transition event, T_{g1}. At temperatures above T_{g1}, the PEI/SiO_2 sample shows only limited mechanical reinforcement, while a dual-T_g response is evident in each of the PEI/Cab-o-sil materials. Incorporation of TS-720

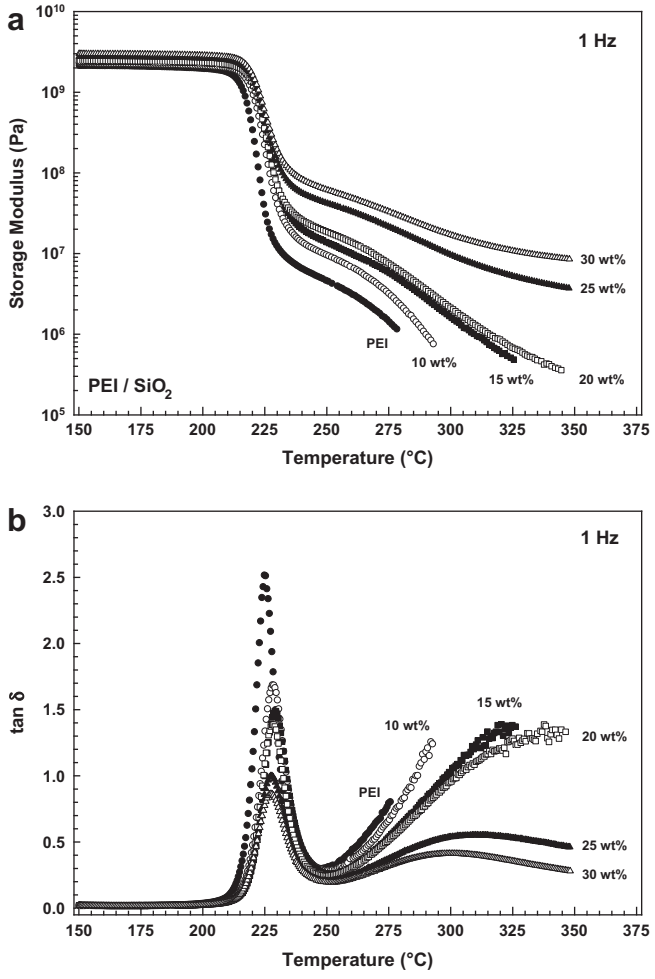

Fig. 3. Dynamic mechanical properties vs. temperature (°C) for PEI/SiO_2 nanocomposites. (a) storage modulus (Pa); (b) tanδ. Frequency of 1 Hz; heating rate of 3 °C/min.

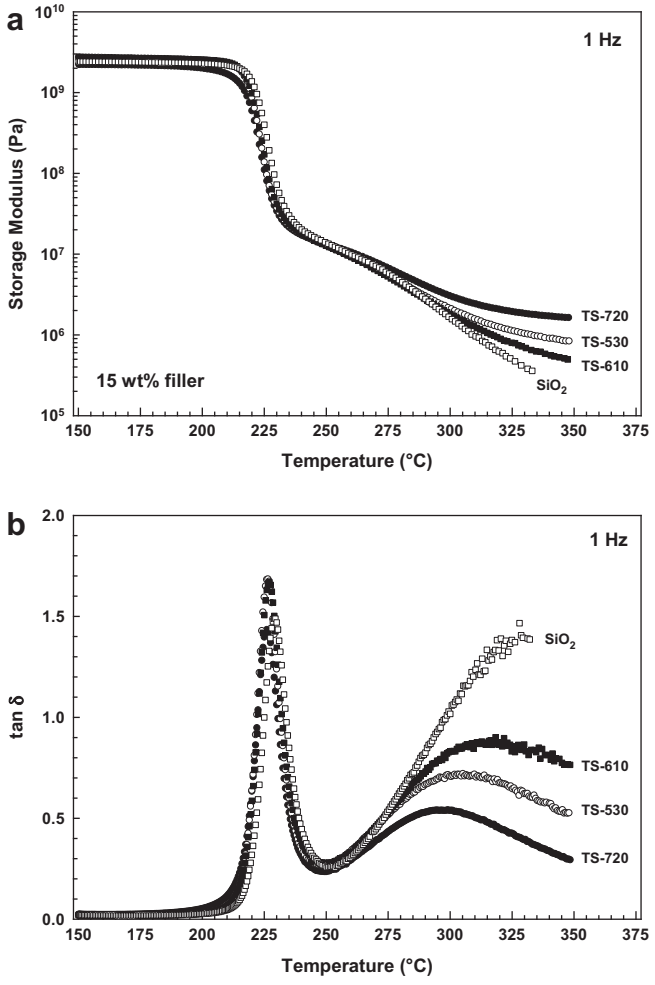

Fig. 4. Dynamic mechanical properties vs. temperature (°C) for PEI nanocomposites with particle loading of 15 wt%: SiO_2; TS-530; TS-610; TS-720. (a) storage modulus (Pa); (b) tanδ. Frequency of 1 Hz; heating rate of 3 °C/min.

particles, which appear to present the most strongly hydrophobic surface, leads to the highest measured value of rubbery modulus above T_{g2}. This correlates with the lowest intensity tanδ peak for the T_{g2} event, suggesting that the PEI/TS-720 composite contains the highest proportion of tightly-bound polymer segments at the particle surface. The loosely-bound segments that are capable of participating in the T_{g2} process are presumably further removed from the TS-720 surface and less constrained as compared to the loosely-bound populations present in the TS-530 and TS-610 composites. As a result, the T_{g2} peak for the TS-720 system is positioned at a lower temperature as compared to the TS-530 and TS-610 composites (see full listing of T_{g1} and T_{g2} values as a function of composition in Table 2).

Representative dynamic mechanical curves of tanδ vs. temperature at various measurement frequencies (PEI/TS-610; 30 wt% filler) are shown in Fig. 5; the range of frequencies is 0.1–30 Hz. Both transitions (i.e., peaks in tanδ) shift to higher temperatures with increasing frequency, consistent with their origin as motional relaxation processes. Plots of log(frequency) vs. reciprocal temperature, based on the measured maxima in tanδ from the isochronal curves, are provided in Fig. 6 for the PEI/TS-610 series. Across the limited range of frequencies accessible with the dynamic mechanical instrument, data for both the T_{g1} and T_{g2} transitions follow the Arrhenius relation, as indicated by the straight-line fits included in the figure. For the T_{g1} glass transition event, the peak temperatures of the composite specimens are shifted to slightly higher values as compared to unfilled PEI (see also Table 2), but all data sets reflect a single apparent activation energy, E_A = 880 kJ/mol. For the T_{g2} relaxation, a much lower activation energy is indicated over the

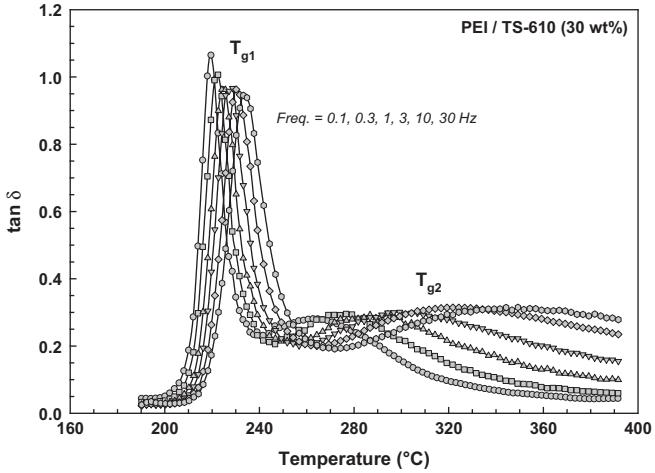

Fig. 5. Dynamic mechanical tanδ vs. temperature (°C) for PEI/TS-610 (30 wt%) nanocomposite. Frequencies of 0.1, 0.3, 1, 3, 10, 30 Hz.

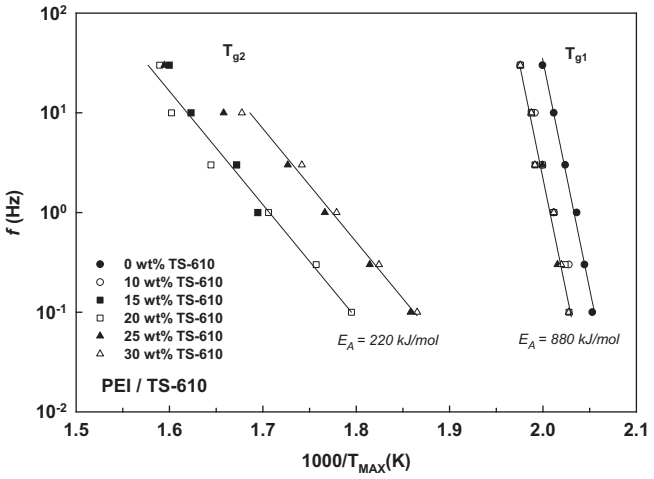

Fig. 6. Arrhenius plots of f (Hz) vs. $1000/T_{MAX}$ (K) for PEI/TS-610 nanocomposites based on maxima in dynamic mechanical tanδ.

various composite loadings ($E_A = 220$ kJ/mol), with the data points positioned according to the observed shifts in T_{g2} to lower temperatures with increased loading. The smaller activation energy encountered for the T_{g2} process is consistent with the results of Tsagaropoulos and Eisenberg [14], who measured E_A values that were 2–3 times lower than the activation energy for the T_{g1} transition at low to moderate filler loadings.

The time–temperature character of the glass transition events in the PEI composites was further explored by the construction of modulus–frequency master curves based on time–temperature superposition [27]. Fig. 7 shows E' vs. ωa_T master curves for the PEI/TS-610 series at a reference temperature of 225 °C, where ω is the applied frequency ($\omega = 2\pi f$, with f expressed in Hz) and a_T is the dimensionless shift factor. The master curves capture the dual relaxation behavior of the PEI composites and the progressive increase in mechanical reinforcement with filler loading. In an effort to quantify the relative breadth of the relaxations, each component was fit to the Kohlrausch–Williams–Watts (KWW) stretched exponential function, with determination of the KWW distribution parameter, β_{KWW} [28]. The value of β_{KWW} can range from 0 to 1, with lower values reflecting broad transitions influenced by intermolecular coupling, crosslinks, particle-polymer interactions and physical confinement. The inset to Fig. 7 shows a representative dual KWW curve fit for the 30 wt% composite. For all composite compositions, the bulk glass–rubber relaxation could be described by a single value of the distribution parameter, $\beta_{KWW} = 0.30$. The higher-temperature transition, corresponding to the relaxation of loosely-bound polymer segments in the vicinity of the particles, broadened with increasing polymer loading: β_{KWW} values for the higher-temperature process were 0.30 for the 10 and 15 wt% samples, 0.20 for the 20 wt% composite, and 0.15 for the 25 and 30 wt% loadings, respectively (PEI/TS-610 series). The low values of β_{KWW} measured at the highest filler loadings reflect the increasingly heterogeneous relaxation environment of the polymer chain segments as influenced by their interactions with the particles, as well as local physical confinement with decreasing overall interparticle distance.

3.3. PMMA composites – dynamic mechanical analysis

In order to assess the generality of the dual-T_g response, a series of PMMA/TS-610 specimens was examined by dynamic mechanical analysis; dual-T_g behavior for the combination of PMMA with native silica (10 and 20 wt%) was previously reported in Ref. [14]. Dynamic mechanical results for the PMMA/TS-610 series are presented in Fig. 8. Unfilled PMMA displays a glass transition centered at 130 °C (peak in tanδ at 1 Hz), and increasing particle loading leads to a strong decrease in the intensity of the tanδ peak, as well as a modest shift in T_g to lower temperatures. A dual-T_g response is indicated only at the highest particle loading examined (30 wt%), with the "T_{g2}" process manifested by an extremely broad maximum in tanδ and a corresponding peak temperature of ~200 °C. The failure to observe dual-T_g character at lower loadings may be a reflection of the lower degree of compatibility inherent to the combination of PMMA with the hydrophobically-modified TS-610, as compared to native SiO_2.

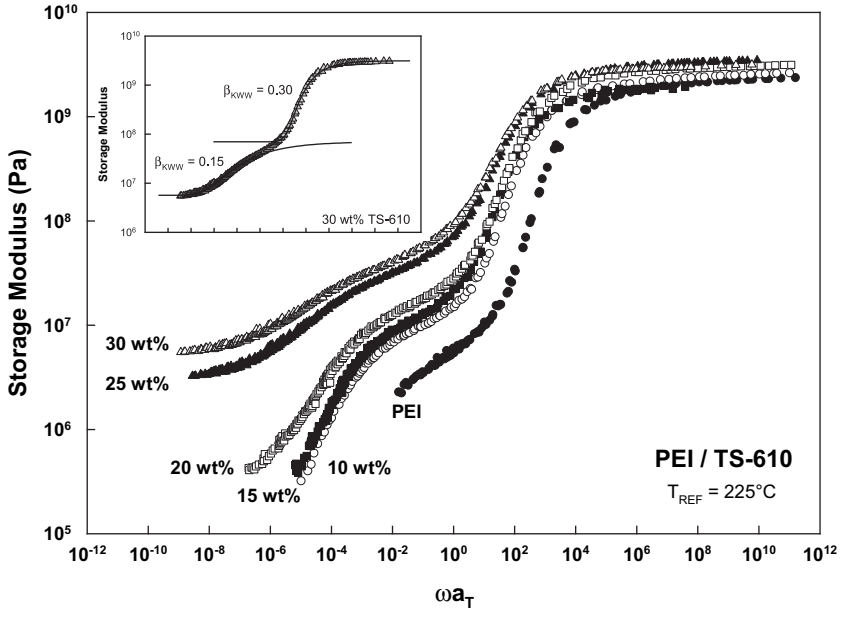

Fig. 7. Time–temperature master curves (E' vs. ωa_T) for PEI/TS-610 nanocomposites. Reference temperature of 225 °C. *Inset*: dual KWW curve fits for 30 wt% TS-610 composite.

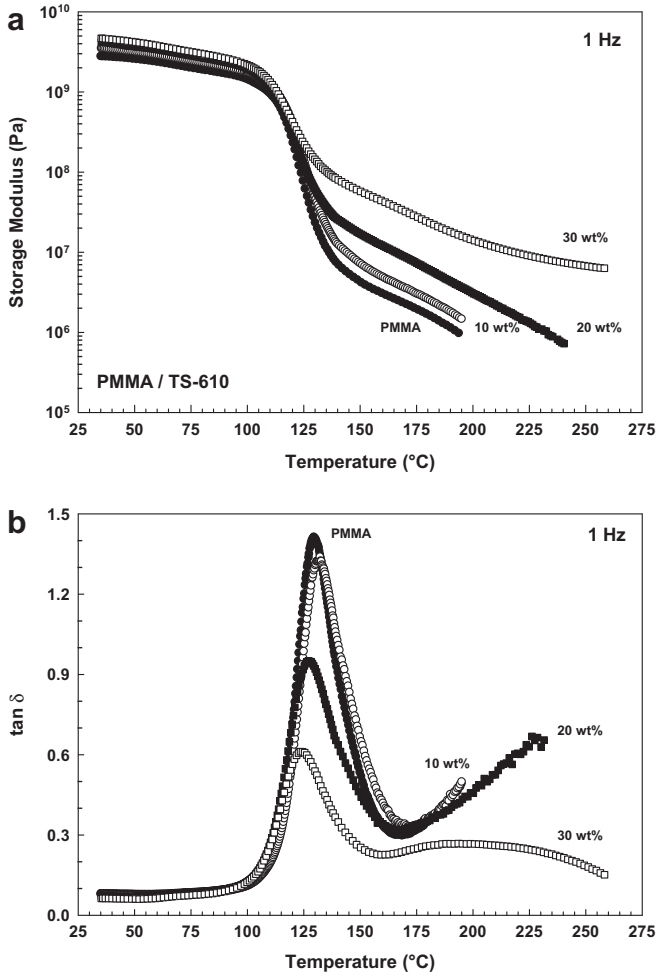

Fig. 8. Dynamic mechanical properties vs. temperature (°C) for PMMA/TS-610 nanocomposites. (a) storage modulus (Pa); (b) tanδ. Frequency of 1 Hz; heating rate of 3 °C/min.

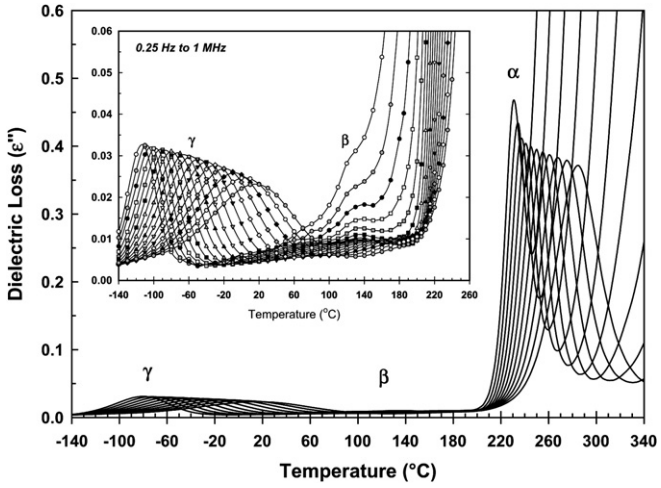

Fig. 9. Dielectric loss (ε'') vs. temperature for unfilled PEI; selected frequencies from 75 Hz to 1 MHz. *Inset*: expanded view of dielectric loss across the sub-glass region (0.25 Hz–1 MHz).

3.4. PEI composites — dielectric spectroscopy

Broadband dielectric measurements can serve as a valuable complement to dynamic mechanical studies for the investigation of sub-glass and glass–rubber relaxation processes in polymer composites, as they provide time–temperature information across an exceptionally wide range of test frequencies (i.e., ≥6–8 orders of

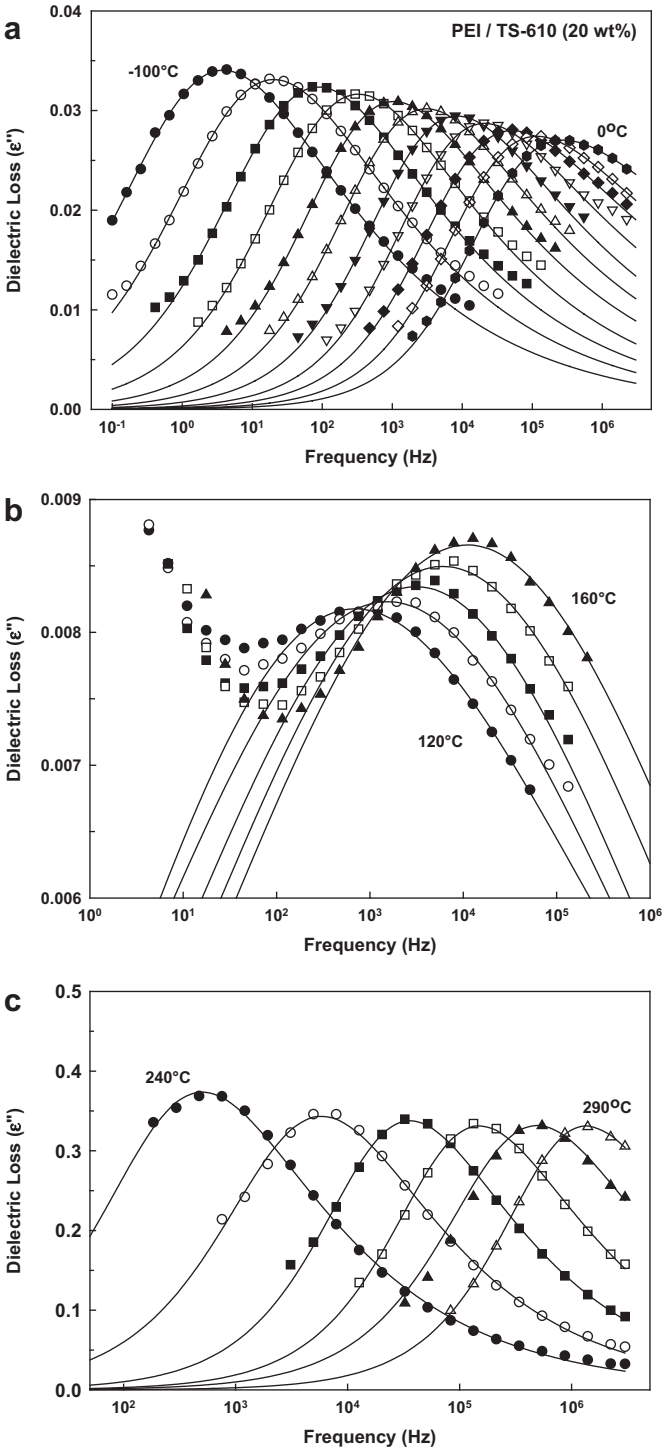

Fig. 10. Dielectric loss (ε'') vs. frequency (Hz) for PEI/TS-610 (20 wt%) nanocomposite. Results are reported at 10 °C intervals; solid curves correspond to HN best-fits. (a) sub-glass γ transition; (b) sub-glass β transition; (c) glass–rubber α transition.

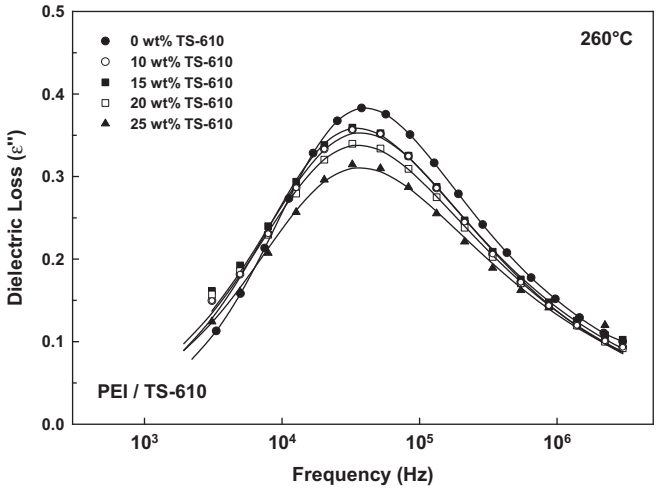

Fig. 11. Dielectric loss (ε'') vs. frequency (Hz) for PEI/TS-610 nanocomposites at 260 °C (glass–rubber relaxation). Solid curves correspond to HN best-fits.

magnitude). Dielectric results for unfilled PEI are plotted as dielectric loss (ε'') vs. temperature in Fig. 9. Three distinct relaxation processes are evident with increasing temperature: the sub-glass γ and β processes, and the glass–rubber α process. At a test frequency of 1 kHz, the corresponding relaxation temperatures are −60 °C (γ), 120 °C (β) and 240 °C (α), respectively. The features encompassed in Fig. 9 are consistent with previous reports on the relaxation characteristics of the PEI thermoplastic [29–32].

Representative plots of dielectric loss vs. frequency at discrete temperatures in the range of the γ, β, and α relaxations are presented for the PEI composites in Fig. 10 (PEI/TS-610; 20 wt% filler). The dielectric dispersions are fit according to the Havriliak–Negami (HN) modification of the Debye equation in order to establish the central relaxation times (τ_{MAX}) associated with each process [33]; details of the analysis are available in Kalakkunnath et al. [34]. A comparison of the α relaxation response for the PEI/TS-610 composites at 260 °C is presented in Fig. 11. The addition of filler particles leads to a systematic decrease in the intensity of the dielectric loss, but the location of the α relaxation is unchanged by the presence of the particles. This outcome is consistent with the results obtained via dynamic mechanical analysis (T_{g1} process), for which the peak position of the bulk polymer relaxation was essentially independent of increasing filler content.

Attempts to detect a second, higher-temperature glass–rubber relaxation process using dielectric relaxation spectroscopy were unsuccessful, owing to ionic conduction and the strong interfacial polarization response encountered in the composite samples at temperatures $> T_{g1}$. In heterogeneous materials above the glass transition, the polarization of mobile charges at interfacial boundaries can lead to contributions to dielectric constant and loss that far exceed the magnitude of the orientational polarizations associated with local and longer-scale segmental motions [35]. This was the case with the PEI- and PMMA-based composites, wherein the high intensity of interfacial polarization effectively masked the detection of possible higher-temperature relaxations associated with a constrained segmental population.

Arrhenius plots based on the dielectric measurements are presented in Fig. 12, with f_{MAX} for each temperature determined from the isothermal HN fits as $f_{MAX} = [2\pi\tau_{MAX}]^{-1}$. For each of the three relaxations, the data indicate no variation as a function of particle loading in the composite. The linear Arrhenius character of the time–temperature data for the γ and β processes is consistent with non-cooperative motions of limited length scale [30]; the apparent activation energies for the sub-glass processes are $E_A = 45$ kJ/mol (γ) and 84 kJ/mol (β), respectively. The invariance of the measured relaxation times with composition suggests that the underlying dipolar reorientations associated with the γ and β transitions are sufficiently localized to remain unperturbed by the presence of the nanoscale particles, even at the highest loadings investigated.

The α relaxation data reported in Fig. 12 correspond to the "T_{g1}" glass transition. Fig. 13 shows the dielectric α relaxation data plotted over a much narrower range of $1/T$, and combined with dynamic mechanical data established from maxima in the loss modulus as a function of temperature. When viewed on this basis, the data again reveal minimal variation in relaxation peak location as a function of particle loading, other than a slight positive shift in

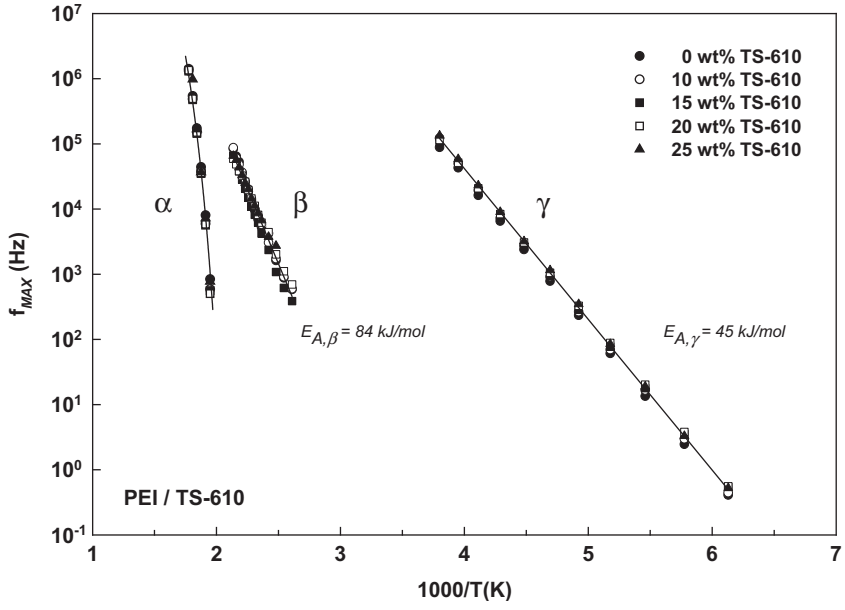

Fig. 12. Arrhenius plots of f_{MAX} (Hz) vs. 1000/T(K) for PEI/TS-610 nanocomposites based on maxima in dielectric loss.

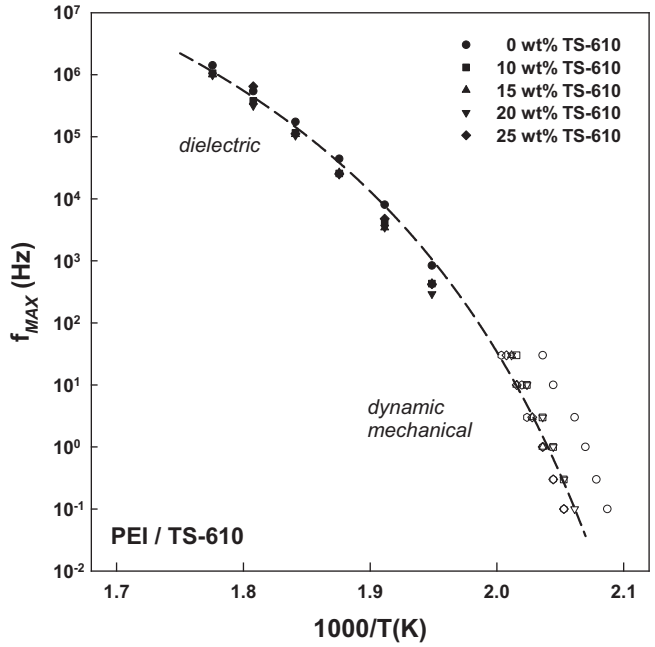

Fig. 13. Arrhenius plots of f_{MAX} (Hz) vs. 1000/T(K) for PEI/TS-610 nanocomposites across the glass–rubber relaxation. Dashed curve represents WLF best-fit. Unfilled symbols correspond to dynamic mechanical measurements; filled symbols correspond to dielectric measurements.

relaxation temperature for the composites as compared to the unfilled PEI resin. The curvature evident in the combined data (when plotted on an Arrhenius basis) is consistent with the underlying cooperative character of the bulk polymer glass–rubber relaxation. Good overall agreement is obtained between the dielectric and dynamic mechanical methods, and the entire data set can be adequately described by a single Williams–Landel–Ferry (WLF) relation [27], where $C_1 = 11.2$, $C_2 = 62$ K and $T_{REF} = 490$ K (relative to a reference frequency of 1 Hz).

3.5. PMMA composites – dielectric spectroscopy

Dielectric studies of PMMA and the PMMA/TS-610 composites were performed to assess the potential influence of nanoparticles

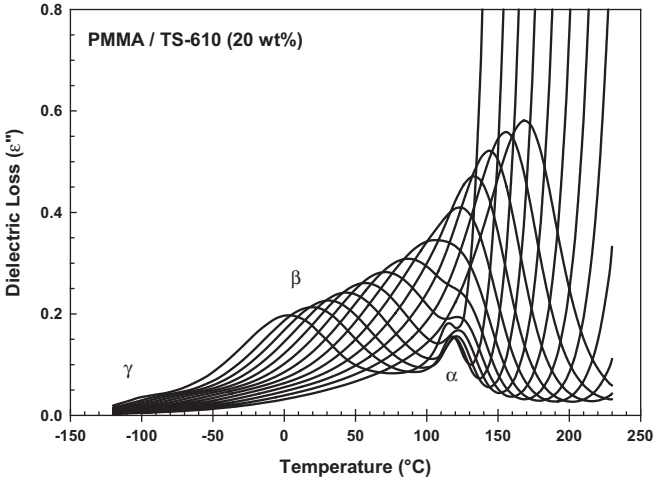

Fig. 14. Dielectric loss (ε'') vs. temperature for PMMA/TS-610 nanocomposite; selected frequencies from 0.5 Hz to 1 MHz.

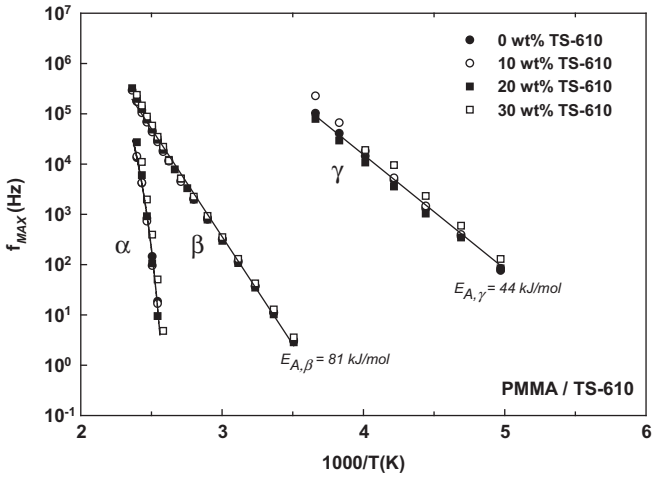

Fig. 15. Arrhenius plots of f_{MAX} (Hz) vs. 1000/T(K) for PMMA/TS-610 nanocomposites based on maxima in dielectric loss.

on the time–temperature relaxation behavior of the PMMA matrix. Representative results (ε'' vs. temperature) for the 20 wt% PMMA/TS-610 composite are presented in Fig. 14 and display three relaxations with increasing temperature, designated γ, β and α, respectively. The molecular origins for the PMMA relaxations are well-established, with the weak γ transition corresponding to isolated rotation of the main-chain methyl group, the β transition corresponding to local ester side-group rotations, and the α transition corresponding to the glass–rubber relaxation [36,37]. At higher temperatures and frequencies, the β and α relaxations merge into a single dielectric dispersion peak. Arrhenius plots for PMMA and the composites are provided in Fig. 15 (dielectric data, only). The γ and β processes show linear Arrhenius behavior and corresponding activation energies that are consistent with the local, non-cooperative origins of these relaxations, with $E_A = 44$ kJ/mol for the γ transition and $E_A = 81$ kJ/mol for the β transition. The α relaxation can be described by the WLF form (see plot). As was the case with the PEI-based formulations, the time–temperature response behavior of the PMMA composites is independent of filler content, and matches the results obtained for the unfilled PMMA resin. Here again, it was not possible to differentiate a potential higher-temperature glass–rubber relaxation event, owing to strong conduction and interfacial polarization in the PMMA composites at temperatures above T_g.

4. Conclusions

The dynamic relaxation characteristics of PEI- and PMMA-based polymer nanocomposites were investigated as a function of nanoparticle loading and surface chemistry. For the PEI composites, four series of specimens were studied based on the inclusion of native SiO_2 particles, as well as commercial particles prepared with hydrophobic surface modifications. Density measurements showed close adherence to volume additivity, especially for the TS-610 and TS-720 particles, indicating minimal entrapment of void volume in the preparation of the composites. Dynamic mechanical measurements revealed a dual-T_g relaxation behavior. The lower temperature transition (T_{g1}) corresponded to the relaxation of bulk, unperturbed polymer segments in the matrix, and was positioned very close to the transition temperature of the unfilled thermoplastic. The higher-temperature transition (T_{g2}) corresponded to the relaxation of loosely-bound chain segments constrained to some degree by their proximity to the particle surface. The location

and intensity of the higher-temperature transition was influenced by the conversion of loosely-bound polymer to tightly-bound polymer at higher particle loadings; the immobilization of some portion of the loosely-bound segments at higher loadings led to a decrease in the intensity of the T_{g2} relaxation event, and a shift in the position of the loss maximum to lower temperatures. The dual-T_g response was well-established in the PEI/Cab-o-sil composites at filler loadings $\geq$ 15 wt%. For the less compatible PEI/SiO_2 combination, a dual-T_g response was observed at loadings $\geq$ 25 wt%.

Dielectric measurements were used to probe the influence of the filler particles on the polymer response across the sub-glass relaxation region, as well as in the vicinity of the glass transition. For both the PEI and PMMA composites, the introduction of nanoscale filler had no effect on the dielectric time–temperature characteristics of the local sub-glass relaxations. The position of the bulk polymer glass transition was also independent of filler content, in agreement with the dynamic mechanical measurements; the combined dynamic mechanical and dielectric data sets were observed to follow a single, cooperative (i.e., WLF) expression for all composite loadings. Efforts to distinguish a second, higher-temperature dielectric glass transition in the composites were unsuccessful, owing to the high level of interfacial polarization response that was encountered.

Acknowledgments

Acknowledgment is made to the Donors of the American Chemical Society Petroleum Research Fund (PRF #45353-AC7) for support of this work. The authors are pleased to recognize the contributions of Matthew A. Borns to the early stages of this study, and the supporting dielectric experiments completed by Michael K. Abney.

References

[1] Vaia RA, Giannelis EP. MRS Bull 2001;26:394–401.
[2] Jordan J, Jacob KI, Tannenbaum R, Sharaf MA, Jasiuk I. Mat Sci Eng A 2005;393:1–11.
[3] Tjong SC. Mater Sci Eng R 2006;53:73–197.
[4] Balazs AC, Emrick T, Russell TP. Science 2006;314:1107–10.
[5] Crosby AJ, Lee J-Y. Polym Rev 2007;47:217–29.
[6] Schaefer DW, Justice RS. Macromolecules 2007;40:8501–17.
[7] Winey KI, Vaia RA. MRS Bull 2007;32:314–22.
[8] Paul DR, Robeson LM. Polymer 2008;49:3187–204.
[9] Jancar J, Douglas JF, Starr FW, Kumar SK, Cassagnau P, Lesser AJ, et al. Polymer 2010;51:3321–43.
[10] Robertson CG, Roland CM. Rubber Chem Tech 2008;81:506–22.
[11] Yim A, Chahal RS, St. Pierre LE. J Colloid Interface Sci 1973;43:583–90.
[12] Reid CG, Greenberg AR. J Appl Polym Sci 1990;39:995–1014.
[13] Tsagaropoulos G, Eisenberg A. Macromolecules 1995;28:396–8.
[14] Tsagaropoulos G, Eisenberg A. Macromolecules 1995;28:6067–77.
[15] Arrighi V, McEwen I, Qian H, Prieto M. Polymer 2003;44:6259–66.
[16] Fragiadakis D, Pissis P, Bokobza L. Polymer 2005;46:6001–8.
[17] Fragiadakis D, Pissis P. J Non-Cryst Solids 2007;353:4344–52.
[18] Chen L, Zheng K, Tian X, Hu K, Wang R, Liu C, et al. Macromolecules 2010;43:1076–82.
[19] Ash BJ, Siegel RW, Schadler LS. J Polym Sci B Polym Phys 2004;42:4371–83.
[20] Bansal A, Yang H, Li C, Cho K, Benicewicz BC, Kumar SK, et al. Nat Mater 2005;4:693–8.
[21] Bansal A, Yang H, Li C, Benicewicz BC, Kumar SK, Schadler LS. J Polym Sci B Polym Phys 2006;44:2944–50.
[22] Rittigstein P, Torkelson JM. J Polym Sci B Polym Phys 2006;44:2935–43.
[23] Takahashi S, Paul DR. Polymer 2006;47:7519–34.
[24] Takahashi S, Paul DR. Polymer 2006;47:7535–47.
[25] Krishnamoorti R. MRS Bull 2007;32:341–7.
[26] G.E. Plastics: Technical Data Sheet for Ultem Resin 1000; 2003.
[27] Ferry JD. Viscoelastic properties of polymers. 3rd ed. New York: John Wiley and Sons; 1980.
[28] Williams G, Watts DC, Dev SB, North AM. Trans Faraday Soc 1971;67:1323–35.
[29] Goodwin AA, Simon GP. Polymer 1996;37:991–5.
[30] Goodwin A, Marsh R. Macromol Rapid Comm 1996;17:475–80.
[31] Bristow JF, Kalika DS. Polymer 1997;38:287–95.
[32] Jenkins MJ. Polymer 2000;41:6803–12.
[33] Havriliak S, Havriliak SJ. Dielectric and mechanical relaxation in materials. Cincinnati: Hanser; 1997.
[34] Kalakkunnath S, Kalika DS, Lin H, Raharjo RD, Freeman BD. Polymer 2007;48:579–89.
[35] Steeman PAM, van Turnhout J. Dielectric properties of inhomogeneous media. In: Kremer F, Schonhals A, editors. Broadband dielectric spectroscopy. Berlin: Springer-Verlag; 2003. p. 495–522.
[36] McCrum NG, Read BE, Williams G. Anelastic and dielectric effects in polymer solids. London: John Wiley and Sons; 1967. reprinted by Dover Publications, 1991.
[37] Hedvig P. Dielectric spectroscopy of polymers. New York: John Wiley and Sons; 1977.